JOURNAL OF MATERIALS SCIENCE **38** (2003) 3619–3628

NaCl-induced accelerated oxidation of 304 stainless steel and Fe-Mn-Al alloy at 900°C

JYH-WEI LEE*
Department of Materials Science and Engineering, National Tsing Hua University, Hsin-Chu, Taiwan, Republic of China

CHAUR-JENG WANG‡
Department of Mechanical Engineering, National Taiwan University of Science and Technology, Taipei, Taiwan, Republic of China
E-mail: cjwang@mail.ntust.edu.tw

JENQ-GONG DUH
Department of Materials Science and Engineering, National Tsing Hua University, Hsin-Chu, Taiwan, Republic of China

The high-temperature corrosion behavior of cold-rolled and annealed 304 stainless steel (304SS) and Fe-29Mn-8Al-2.5Si-2Cr-0.74C alloy coated with 0.002 g cm^{-2} NaCl initially were studied at 900°C in air. The corrosion kinetics of the two alloys follow the parabolic rate law. The initial NaCl coating accelerates oxidation of these alloys by oxychlorination and chlorination/oxidation cyclic reactions, and catalytic actions of chloride or chlorine are thought to be the principal causes. A bulky, layered scale as well as some intergranular attack is noted on the annealed 304SS, and intergranular attack distributes over the alloy substrate of the cold-rolled 304SS during a 144 h exposure. With the formation of a compact Al_2O_3 scale to decrease further chlorine attack, the corrosion resistance of Fe-Mn-Al alloy is superior to that of 304SS in this study.

1. Introduction

Sodium chloride is one of the main components of seawater. The evaporated sea salt in air will deposit directly on materials, or will mix with Na_2SO_4 produced by reactions between impurities contained in the fuel and ashes and adhere to the component surfaces of a turbine engine of a ship, an aircraft, or other seashore industrial equipment, resulting in hot corrosion of materials. It has been reported that the corrosion loss of Fe-Ni-Cr alloys caused by the presence of NaCl at high temperatures is 30 to 120 times higher than that without NaCl presence [1].

Owing to the high volatilization and ambient temperature hydration of chloride, the identification of metal chlorides generated by chlorination in chlorine-containing environments is not an easy task [2]. In general, it is agreed that the corrosion reaction induced by NaCl begins with oxychlorination in which metals react with oxygen and NaCl, releasing chlorine. For Cr-containing alloys, such as Ni-Cr-Al alloy, the chlorine ions then enter into the Cr_2O_3 lattice and increase rates of cation diffusion in Cr_2O_3, producing a coarse and crystalline Cr_2O_3 layer, which grows rapidly [2]. In addition, the chlorine might attack the alloy substrate to form metal chlorides, which act as intermediate compounds for the self-sustaining reactions of chlorination/oxidation [3, 4]. However, for Al_2O_3-forming alloys, our previous study indicated that Fe-31Mn-9Al-0.89C coated with 0.002 g cm^{-2} NaCl showed excellent high temperature corrosion resistance at 850°C by forming a protective Al_2O_3 scale [5]. Due to the disputed mechanism of the above reactions induced by NaCl, as well as the ambiguous effects on thermal mechanical treatment for alloys [6–8], the purpose of this research was to study the corrosion mechanisms of Al_2O_3- and Cr_2O_3-forming alloys in the NaCl-induced accelerated oxidation of materials, and the effects of thermal mechanical treatment were also explored. Cold-rolled and annealed 304 stainless steel (hereafter referred as "304SS") as well as a Fe-29.2Mn-8.5Al-2.5Si-2.2Cr-0.74C alloy (hereafter referred as "Femnal") were tested at 900°C with 0.002 g cm^{-2} NaCl deposits. The corrosion behavior of these alloys was investigated through kinetics evaluation and morphological examination, and a hypothetical mechanism by which metals could be oxidized quickly in the presence of NaCl has been proposed.

Present address: Department of Mechanical Engineering, Tung Nan Institute of Technology, Taipei, Taiwan, Republic of China.
‡*Corresponding address*: National Taiwan University of Science and Technology, Department of Mechanical Engineering, 43, Keelung Road, Section 4, Taipei 10617, Taiwan, Republic of China.

TABLE I The chemical composition (wt%) of alloys employed in this study

Alloy	Cr	Ni	Si	Mn	Al	C	Fe
304SS	18.01	8.11	0.42	0.96	–	0.07	Bal.
Femnal	2.18	–	2.46	29.18	8.44	0.74	Bal.

2. Experiment procedure

The chemical compositions of the alloys used in this study are listed in Table I. The cold-rolled 304SS specimen was designated as "304R" and the other 304SS specimens, annealed for 30 min at 950°C, were designated as "304A". An as-cast ingot (150 × 70 × 20 mm) of Femnal was homogenized at 1100°C for 4 h. Specimens of the two alloys were cut to the dimension of 18 × 20 × 2 mm by a water-cooled cutting machine. Specimens were ground through 1200-grit SiC paper and then cleaned, dried, weighed and sprayed uniformly with fine NaCl up to 0.002 g cm^{-2} prior to testing. Before spraying with NaCl, platinum was used as a marker spot-welded on the surface of some specimens. Each NaCl-coated specimen was laid in a crucible under a lid. Crucibles with specimens were stored in a stainless steel container and heated in a box furnace (temperature variation range ±6°C) in air atmosphere at 900°C for times between 1 and 144 h. To compare the effect of NaCl on the alloys, some specimens were used to demonstrate a simple oxidation without NaCl deposits.

In addition, alumina plates with 0.002 g cm^{-2} NaCl deposited were oxidized in static air at 900°C for different times to investigate the volatilization of molten NaCl. The volatilization rate of NaCl was about 0.009 g cm^{-2} h^{-1}, indicating that the initial NaCl coating in this study would deplete from the specimen surface within 15 min. According to the previous study [9], the volatilization behavior of molten salt at 850°C followed a linear rate law during the first 20 min. In addition, a further examination using energy-dispersive spectrometry was employed in this study to clarify the existence of coated NaCl, revealing that no NaCl could be observed on alloy surface after 15 min test.

3. Results

3.1. Corrosion kinetics

The corrosion kinetics of the alloys are shown with plots of weight gains versus square root of time in Fig. 1, revealing that weight gain kinetics obey the parabolic rate law. The parabolic rate constants listed in Table II are calculated based on the corrosion kinetics data. For the calculation of the parabolic rate constants on 304SS, time intervals were taken from 1 to 49 h due to the fact that internal attack had penetrated through the 304R specimens after 144 h test. The parabolic rate constants of 304SS including 304A and 304R are about 1×10^{-8} g^2 cm^{-4} sec^{-1}, whereas the oxidation rate of Femnal is only 7.16×10^{-11} g^2 cm^{-4} sec^{-1}, which is 2.2 orders of magnitude lower than that of 304SS at 900°C, indicating that high temperature corrosion resistance of the Al_2O_3-forming Femnal is obviously better than that of the Cr_2O_3-forming 304SS. Table III shows the weight gain values with and without NaCl deposits exposed for 25 h, revealing that the presence of NaCl plays a significant role in accelerating oxidation of the alloys, especially for 304SS.

TABLE II Parabolic rate constants kp (g^2 cm^{-4} sec^{-1}) of alloys at 900°C

Specimen	kp	Log (kp)	Time interval (h)
304A	1.36×10^{-8}	−7.87	1–49
304R	1.07×10^{-8}	−7.97	1–49
Femnal	7.16×10^{-11}	−10.14	1–144

TABLE III The weight gain (g cm^{-2}) values of the alloys exposure at 900°C for 25 h

Specimen	Simple oxidation	Hot corrosion
304A	7.8×10^{-4}	4.1×10^{-2}
Femnal	2.1×10^{-3}	7.4×10^{-3}

3.2. Microstructures and phase constitution

3.2.1. 304 stainless steel

In general, most of the external scales will peel off during cooling for the two alloys, and black large-granule Fe_2O_3 particles are found on the inner wall of crucible containing 304SS after tests. Cross-sectional optical micrographs of 304SS oxidized for 144 h are shown in Fig. 2. A thick and layered scale as well as some intergranular attack are noted on 304A, and intergranular attack can be found obviously even after 1 h of testing and has distributed throughout the alloy substrate of 304R after 144 h exposure.

A cross-sectional SEI micrograph of 304R exposed for 1 h and the corresponding X-ray maps is shown in Fig. 3, revealing that the outer scale is rich in iron and the inner scale is rich in chromium, while some

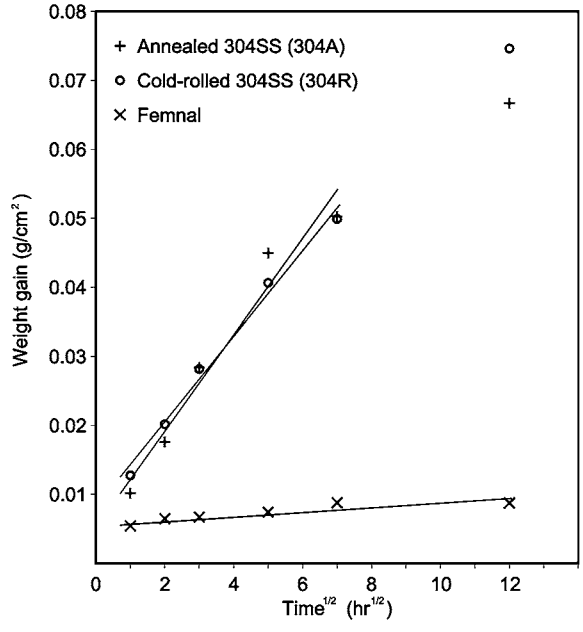

Figure 1 Corrosion kinetics of alloys with 0.002 g cm^{-2} NaCl deposits initially oxidized at 900°C in air.

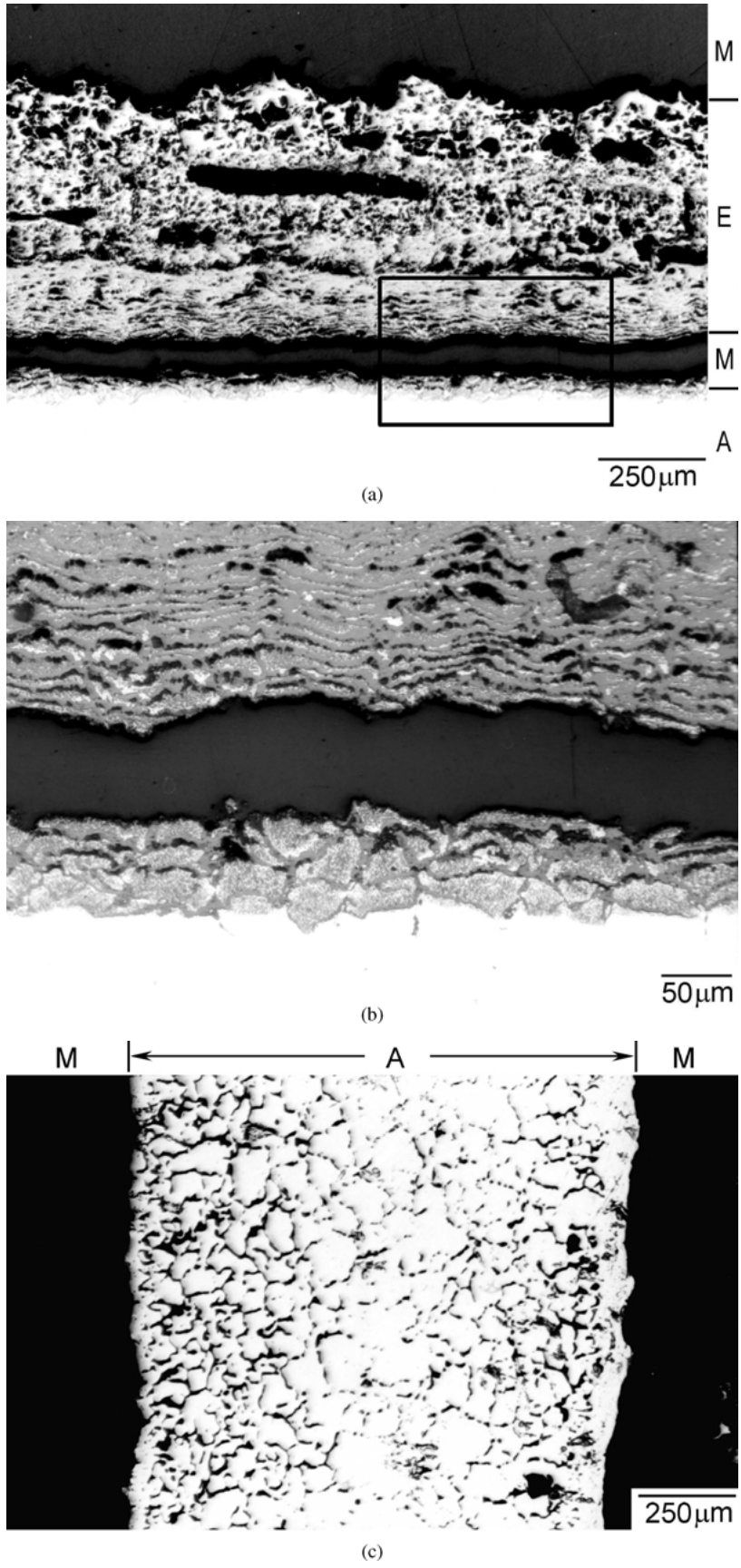

Figure 2 Optical micrographs of the unetched cross-section of 304SS with 0.002 g cm^{-2} NaCl deposits initially oxidized at 900°C in air for 144 h. (a) 304A, (b) high magnification of (a), (c) 304R (external scale spalled). (M: Mounting material, E: External scale, A: the alloy substrate).

chlorides are found in the internal pores. XRD analysis shows that the outer scale consists of mostly Fe_2O_3 and Fe_3O_4, while Cr_2O_3 and minor $NiCl_2$ and $NiCl_2 \cdot 4H_2O$ were detected in the scale/substrate interface. The formation of $NiCl_2 \cdot 4H_2O$ might result from hydration of $NiCl_2$. In addition, the internal pores in the inner part of the alloy substrate, as can be seen in Fig. 4, were depleted in both Fe and Cr, while chlorides concentrated in this region, where the presence of $NiCl_2$ had been verified by XRD analysis.

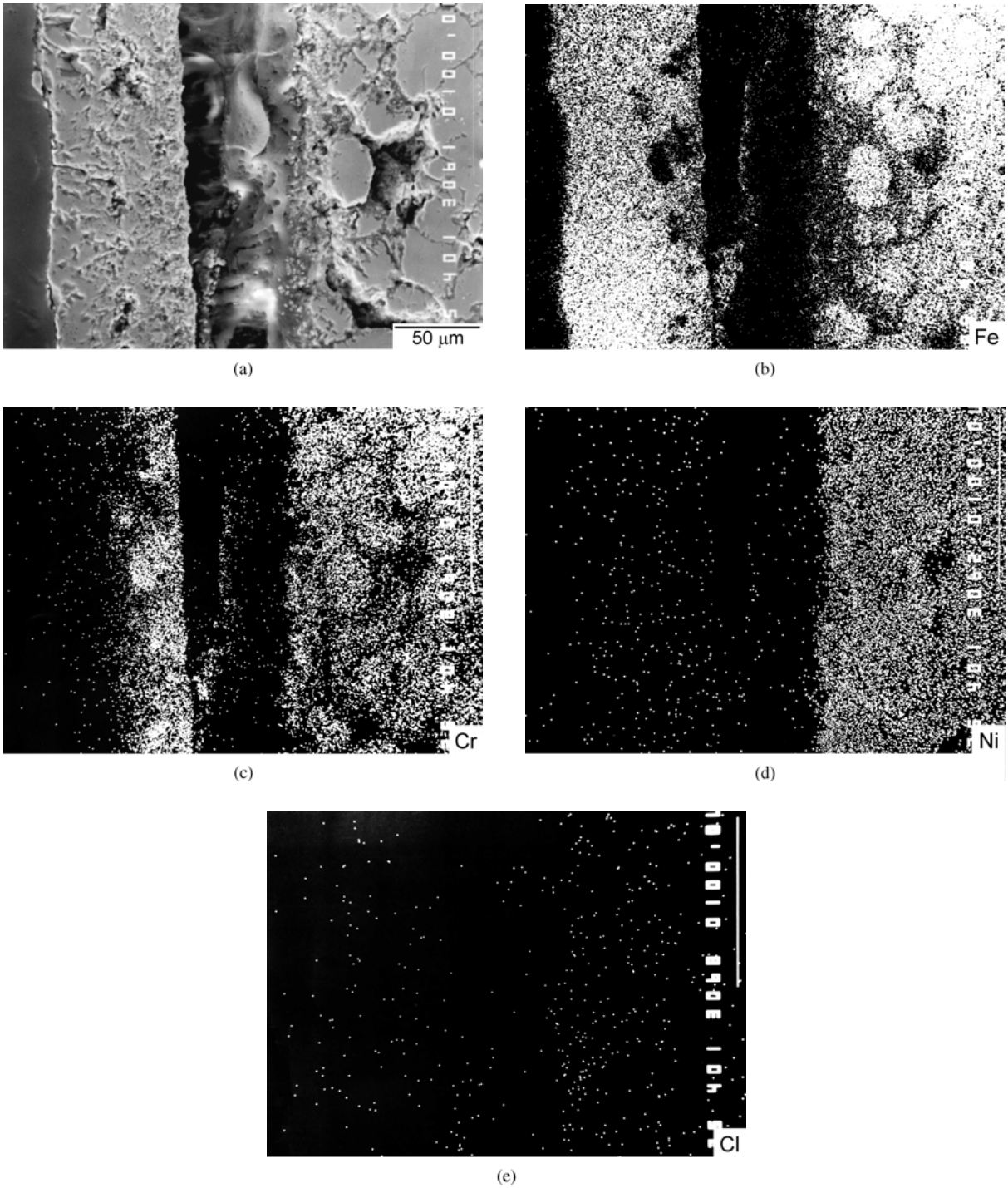

Figure 3 (a) Cross-section of scales and intergranular attack formed on 304R corroded at 900°C for 1 h and X-ray maps of (b) Fe, (c) Cr, (d) Ni, (e) Cl.

Some marker studies were performed to determine the reaction mechanism of the alloys. After optical microscope examination, the platinum marker was found at the innermost scale of the two alloys. Compared with the elemental X-ray maps in Fig. 3, it suggested that the formation of external scale resulted mainly from outward diffusion of cations (iron and chromium), while the inward diffusion of chlorine contributes to the internal attack of subscale.

3.2.2. Femnal alloy

For the Femnal alloy, there were small, thin, black scale spalls during cooling, regardless of testing time. The surface of the alloy substrate is brightly luminescent, which can be observed after scale spalling. A typical cross-sectional optical micrograph of the Femnal alloy with NaCl coating exposed for 144 h is shown in Fig. 5, revealing that a thin and spalled scale is formed. Fig. 6 shows a cross-sectional SEI micrograph of the specimen tested for 25 h and X-ray maps. It is apparent that aluminum accumulates in the inner scale and forms a thin and dense layer, while some chromium carbides are dispersed in the alloy substrate [10]. XRD analysis of the scale reveals that the outer scale primarily consists of Mn_2O_3, $(Mn, Fe)_3O_4$ and minor $MnAl_2O_4$, while the inner scale is covered with Al_2O_3 as well as some $MnAl_2O_4$ and SiO_2.

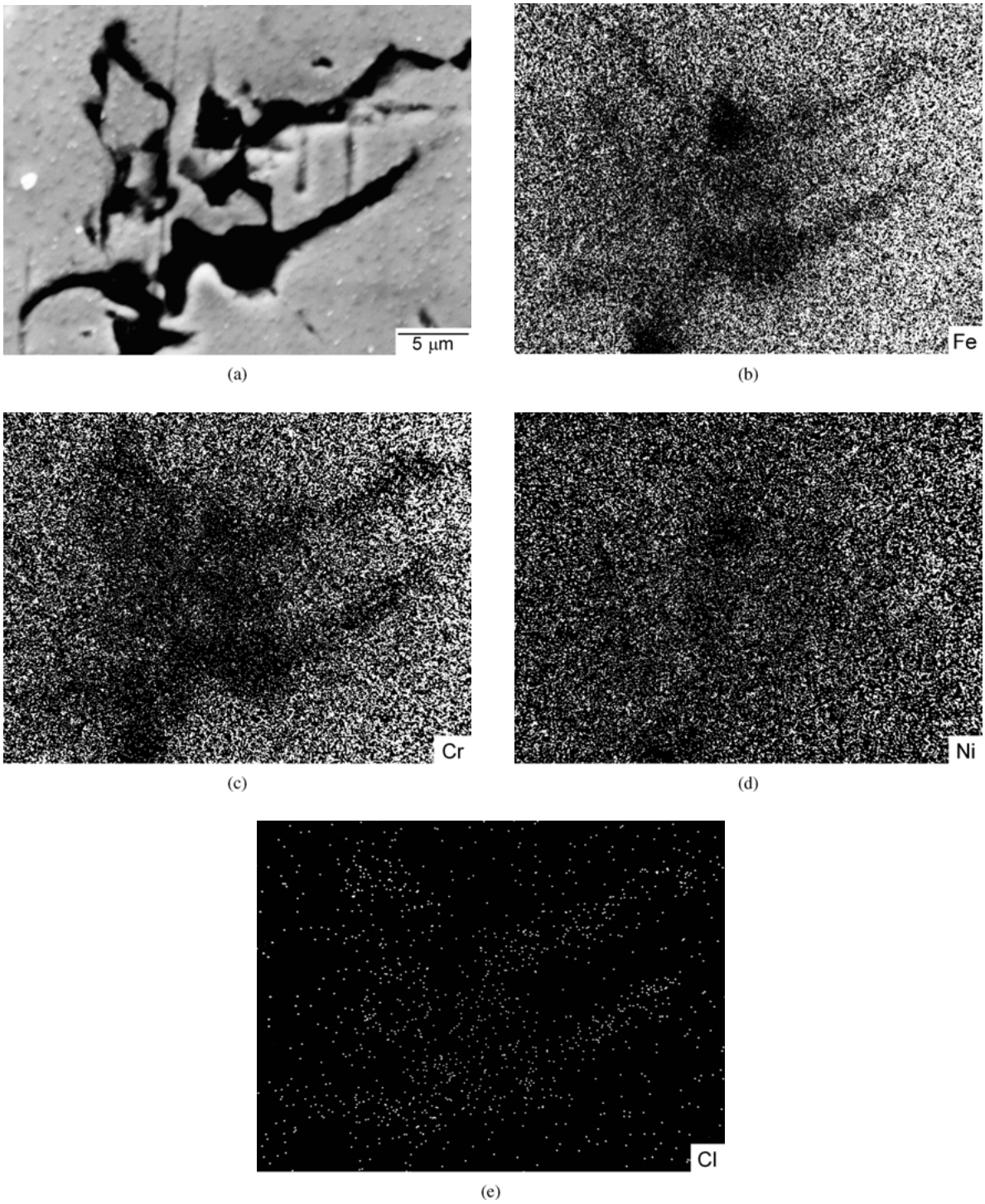

Figure 4 (a) SEM micrograph of internal pores in the alloy substrate of 304R corroded at 900°C for 1 h and X-ray maps of (b) Fe, (c) Cr, (d) Ni, (e) Cl.

4. Discussion

4.1. 304 stainless steel

In the initial stage of heating up to 900°C, solid NaCl will melt due to the fact that the melting point of NaCl is 801°C, and some oxides will form on the surface of the specimen. Misra and Sivakumar [11] reported that the molten NaCl could penetrate this oxide scale. The corrosion attack by a molten salt is particularly deleterious. The transport of cations and anions is increased in the molten salt. In addition, the molten salt may not be a simple compound but most likely a eutectic melt. When the eutectic involves the parent metal of the alloy, severe grain boundary attack of the alloy is to be expected. In NaCl-induced accelerated oxidation, the reaction is generally recognized to be initialized by oxychlorination when metals react with NaCl and oxygen [2]. According to the calculation of thermodynamic data [12, 13], the possible oxychlorination reactions of metals (Cr or Fe) with sodium chloride and dissolved oxygen are listed below:

$$Cr + 2NaCl_{(l)} + 2O_2 = Na_2CrO_4 + Cl_2$$
$$\Delta G = -244.8\,\text{KJ} \quad (1)$$

$$2Cr + 4NaCl_{(l)} + 2O_2 = CrO_2Cl_2 + 2Na_2O$$
$$\Delta G = -280.5\,\text{KJ} \quad (2)$$

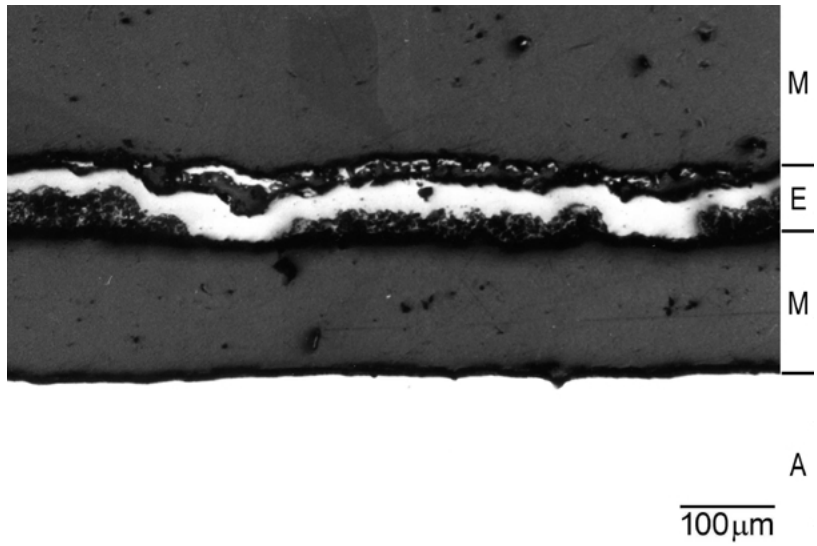

Figure 5 The typical morphology of a Femnal alloy corroded at 900°C for 144 h. (M: Mounting material, E: External scale, A: the alloy matrix).

$$2Cr + 2NaCl_{(l)} + 2O_2 = Cr_2O_3 + Na_2O + Cl_2 \quad \Delta G = -457.6\,KJ \quad (3)$$

$$2Fe + 2NaCl_{(l)} + 2O_2 = Fe_2O_3 + Na_2O + Cl_2 \quad \Delta G = -157.7\,KJ \quad (4)$$

Cr_2O_3 or Fe_2O_3 can react with Na_2O derived from the above reactions to form a complex according to Equation 5.

$$M_2O_3 + Na_2O = NaMO_2 \quad (M = Cr \text{ or } Fe) \quad \Delta G < 0 \quad (5)$$

However, a reaction where Ni reacts with sodium chloride and oxygen to form nickel oxide is highly improbable due to the large positive free energies of formation. Therefore, nickel in 304SS shows noble character in the initial stage of corrosion.

$$Ni + 2NaCl_{(l)} + O_2 = NiO + Na_2O + Cl_2 \quad \Delta G = +227.9\,KJ > 0 \quad (6)$$

A schematic representation of the reactions, product formation, and the distribution of partial pressure of oxygen and chlorine is proposed in this study as shown in Fig. 7. The partial pressure of oxygen gradually declines from the surface of molten salt to the alloy surface in the initial stage of NaCl existence, and the same trend can be hypothesized if the activity of oxygen in the outer scale is higher than in the inner after NaCl depletion. Parts of chlorine released by the above reactions, Equations 1, 3 and 4, escape to the atmosphere and the rest attack the alloy resulting in chlorination, forming $FeCl_{2(l)}$, $CrCl_{2(l)}$, and $NiCl_{2(s)}$ according to Equations 7–9 in places with lower activity of chlorine such as the inner subscale, while $FeCl_{3(g)}$ and $CrCl_{3(s)}$ can be produced according to Equations 10 and 11 in places with higher activity of chlorine, such as the molten salt/substrate interface.

$$Fe + Cl_2 = FeCl_{2(l)} \quad \Delta G = -207.1\,KJ \quad (7)$$

$$Cr + Cl_2 = CrCl_{2(l)} \quad \Delta G = -251.3\,KJ \quad (8)$$

$$Ni + Cl_2 = NiCl_{2(s)} \quad \Delta G = -133.7\,KJ \quad (9)$$

$$2Fe + 3Cl_2 = 2FeCl_{3(g)} \quad \Delta G = -457.8\,KJ \quad (10)$$

$$2Cr + 3Cl_2 = 2CrCl_{3(s)} \quad \Delta G = -590.7\,KJ \quad (11)$$

Due to the fast volatilization rate of NaCl as mentioned above, the activity of oxygen on the alloy surface gradually increases. Chlorides such as $FeCl_{3(g)}$ will vaporize to the atmosphere as indicated in Table IV, while

TABLE IV The thermal properties of various chlorides[12,14]

Chlorides[a] (x)	Melting point (°C)	Boiling point (°C)	Vapor pressure at 900°C (atm)	Dissociation pressure at 900°C (atm)
$NiCl_{2(s)}$	Sublimation	987	0.27×10^{-0}	1.12×10^{-6}
$FeCl_{3(g)}$	315	319	–	1.60×10^{-7}
$CrCl_{3(s)}$	Sublimation	945	0.37×10^{-0}	1.70×10^{-9}
$FeCl_{2(l)}$	677	1026	0.61×10^{-0}	5.96×10^{-10}
$CrCl_{2(l)}$	815	1300	4.13×10^{-3}	6.45×10^{-12}
$SiCl_{4(g)}$	−68	58	–	(4.59×10^{-12})
$MnCl_{2(l)}$	650	1190	2.93×10^{-2}	8.30×10^{-16}
$AlCl_{3(g)}$	193	182	–	3.20×10^{-16}
$NaCl_{(l)}$	801	1465	2.93×10^{-3}	1.13×10^{-27}

[a](x) indicates the state of chlorides at 900°C.

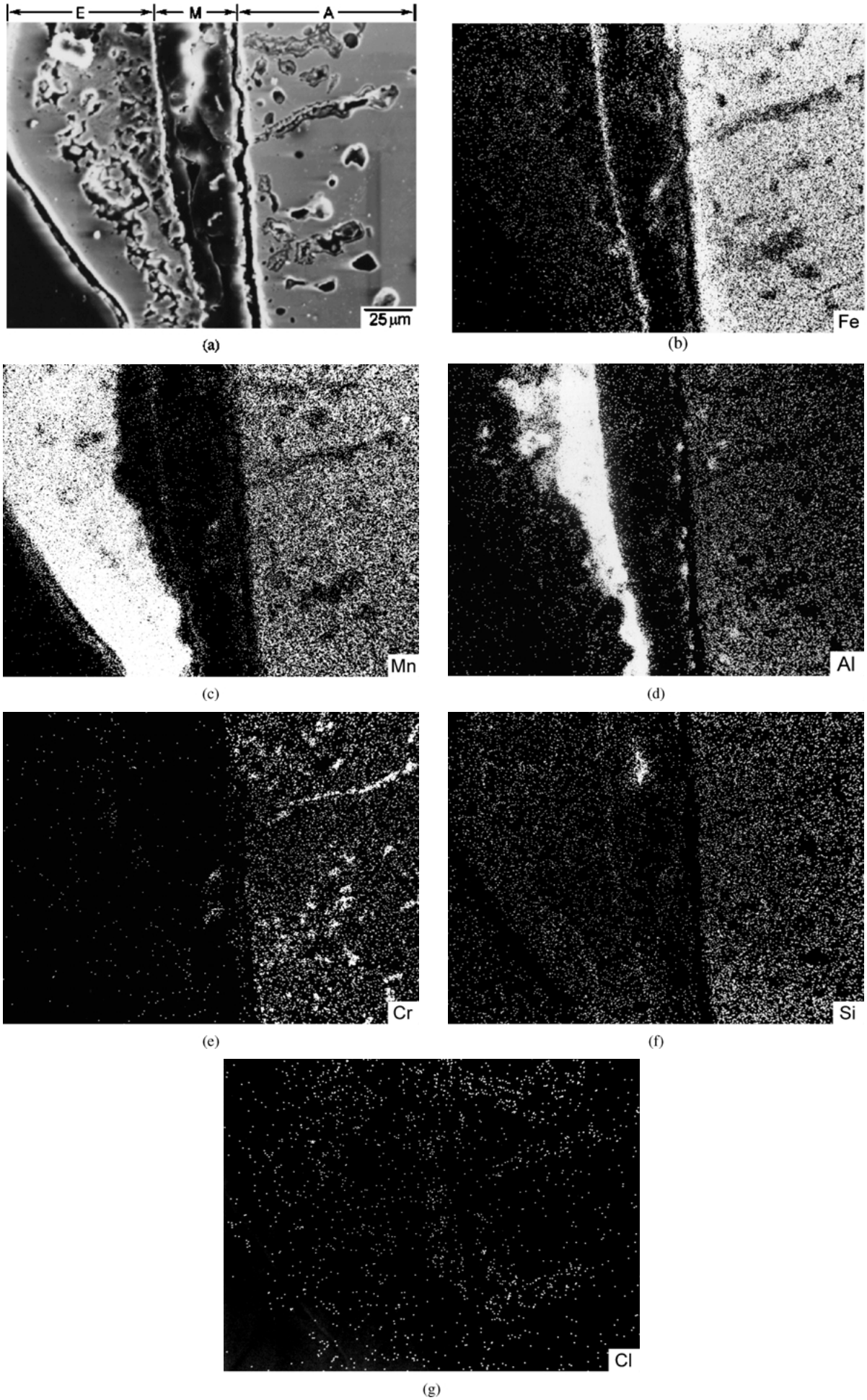

Figure 6 (a) Cross-sectional SEI micrograph of Femnal corroded at 900°C for 25 h and X-ray maps of (b) Fe, (c) Mn, (d) Al, (e) Cr, (f) Si, (g) Cl.

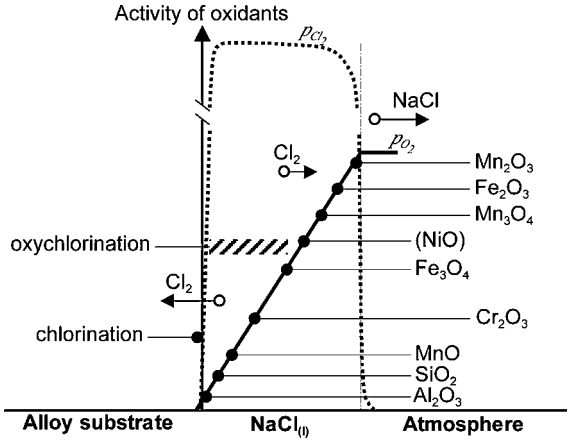

(a)

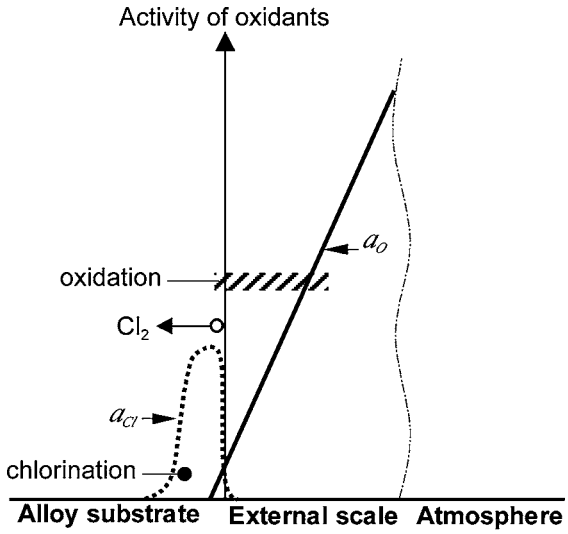

(b)

Figure 7 Schematic representation of the reactions, product formation, and the distribution of partial pressure of oxygen and chlorine during NaCl-induced accelerated oxidation of alloys. (a) the initial oxychlorination as $NaCl_{(l)}$ is still existent. (b) the dominated chlorination/oxidation cyclic reaction when the deposited NaCl was depleted.

$FeCl_{2(l)}$, $NiCl_{2(s)}$, and $CrCl_{3(s)}$ with high vapor pressure could volatilize outward, readily. As these chlorides encounter an area with essential activity of oxygen that enables the onset of oxidation, reactions between metal chlorides and oxygen take place.

$$4FeCl_{3(g)} + 3O_2 = 2Fe_2O_3 + 6Cl_2 \qquad \Delta G = -124.6\,\text{KJ} \quad (12)$$

$$4FeCl_{2(l)} + 3O_2 = 2Fe_2O_3 + 4Cl_2 \qquad \Delta G = -211.7\,\text{KJ} \quad (13)$$

$$3FeCl_{2(l)} + 2O_2 = Fe_3O_4 + 3Cl_2 \qquad \Delta G = -120.3\,\text{KJ} \quad (14)$$

$$2FeCl_{2(l)} + O_2 = 2FeO + Cl_2 \qquad \Delta G = +37.8\,\text{KJ} \quad (15)$$

$$4CrCl_{3(s)} + 3O_2 = 2Cr_2O_3 + 6Cl_2 \qquad \Delta G = -458.7\,\text{KJ} \quad (16)$$

$$4CrCl_{2(l)} + 3O_2 = 2Cr_2O_3 + 4Cl_2 \qquad \Delta G = -635.0\,\text{KJ} \quad (17)$$

TABLE V The dissociation pressure of various oxides at 900°C[12,13]

Oxide	Dissociation pressure (atm)
Mn_2O_3	2.70×10^{-1}
Fe_2O_3	1.40×10^{-7}
Mn_3O_4	3.46×10^{-9}
NiO	1.01×10^{-12}
Fe_3O_4	3.44×10^{-15}
FeO	1.72×10^{-17}
Cr_2O_3	4.50×10^{-25}
MnO	2.32×10^{-27}
SiO_2	7.89×10^{-32}
Al_2O_3	2.12×10^{-39}

$$2NiCl_{2(s)} + O_2 = 2NiO + 2Cl_2 \qquad \Delta G = -2.0\,\text{KJ} \quad (18)$$

As can be seen in Equation 18, the Gibbs free energy of the reaction between $NiCl_2$ and oxygen is nearly zero, indicating that if the partial pressure of oxygen is lower than that of chlorine, $NiCl_{2(s)}$ will be stable.

Due to the high dissociation pressure of Fe_2O_3 as shown in Table V, reactions of iron chloride and oxygen according to Equations 12 and 13 will proceed in places with higher partial pressure of oxygen, such as outer scale. Volatilized $FeCl_{3(g)}$ diffused outward through the non-protective scale will react with oxygen to form Fe_2O_3 on the inner wall of the crucible [15]. Thus, black large-granular Fe_2O_3 can be commonly found in the crucible containing 304SS specimens after high-temperature corrosion in this study. On the other hand, because the Cr_2O_3 scale, which is formed near the specimen's surface with lower partial pressure of oxygen is partly generated by the reactions between chromium chloride and oxygen, it shows loose and discontinuous characteristic as indicated in Figs 2 and 3.

When the NaCl on the specimen's surface is depleted by volatilization and oxychlorination, the provision of chlorine from molten salt ceases. Nevertheless, chlorine gas released by the above reactions could be trapped in the alloy substrate after external scale gradually healed and might continue to react with the metals, as shown in Fig. 4e.

The rate-controlling layer on this alloy is probably Cr_2O_3. However, as mentioned above, Cr_2O_3 scale formed on 304SS is not compact due to the reaction of chromium chloride with oxygen and the lattice defect concentration in the oxide may be increased by chlorine ion doping. Therefore, the rapid outward diffusion of iron and chromium in the alloy substrate leads to the formation of a thick scale of more than 500 μm thickness after 144 h exposure as shown in Fig. 2a. Both iron and chromium outward diffusion result in increasing the nickel activity in this region, and the possibility of forming $NiCl_{2(s)}$ also increases. According to XRD analysis, $NiCl_2$ can be detected in the alloy substrate in this study, implying that chlorine concentration is higher than oxygen beneath the external scale, and under this condition $NiCl_2$ tends to be stable.

For the effect of thermo-mechanical pretreatment on the corrosion morphology of alloys, Seybolt [7]

reported that no different behavior was noted in salt-oxygen corrosion of the Ni-20Cr alloys no matter whether pre-annealing is conducted or not, while Lai [8] indicated that corrosion attack was observed only on the cold-worked area of Ni-Cr-Fe alloy immersed in a molten $CaCl_2$-NaCl salt bath for a long time. Seybolt [7] further proposed a reaction mechanism such that molten salt could penetrate through pores and surface defects by capillary effect and attack the alloy substrate. Even though the test temperature 900°C is lower than the annealing temperature (1040°C) of the 304SS [16], the exothermic effect caused by both chlorination and oxidation might induce the annealing of the alloy substrate during tests. For example, as shown in Fig. 3a, the isotropic grain shape reveals that the alloy substrate has been recrystallized after exposure for 1 h. Recrystallization occurs by the nucleation and growth of new grains. Some impurities such as chlorides may tend to pile up at grain boundaries during recrystallization. As compared with the annealed and cold-rolled specimens in Fig. 2a and c, it is found that the cold-rolled specimen is penetrated by the intergranular attack. However, the corrosion kinetics of two specimens with different pre-treatments is similar as can be seen in Fig. 1, implying that the thermo-mechanical pretreatment only affects the morphology and depth of corrosion attack. For the cold-rolled 340R, the chlorides concentrated at the grain boundaries during recrystallization proceed accelerated intergranular attack, while some intergranular attack is found on the annealed 304A as shown in Fig. 2a and b.

Though the deposited NaCl is depleted, chlorine or chlorides at the grain boundaries will still attack the alloy. The alloying elements are corroded gradually in the way of chlorination/oxidation cyclic reactions, or they may be dissolved into molten chlorides and then be oxidized [7]. As corrosion progresses, grain boundary adjacent to the scale gradually gets wide and grain size becomes shrunk and thin, and the plate-like grain is oxidized to become scale finally. Therefore, as shown in Fig. 2b, a typical morphology of a multi-layered scale formed in the innermost scale is revealed after high temperature corrosion for 144 h.

4.2. Femnal alloy

With adequate amounts of aluminum content to form a protective alumina scale, the Femnal alloys have excellent high-temperature oxidation resistance [5, 17]. Silicon additions of up to 2% prevent the selective oxidation of manganese and enhance oxidation resistance and strength. The resulting austenitic Fe-Mn-Al-Si alloys show promising oxidation and corrosion resistance [17]. In this study, high-temperature corrosion resistance of Femnal alloy is superior to that of 304SS at 900°C as indicated in Tables II and III.

In general, the hot corrosion behavior of NaCl-deposited Femnal alloy is similar to that of 304SS. Oxychlorination in the initial stage and the following steady state chlorination/oxidation cyclic reactions are also noted. The possible oxychlorination reactions and the thermodynamically calculated results are listed as follows.

$$2Al + 2NaCl + 2O_2 = Al_2O_3 + Na_2O + Cl_2 \quad \Delta G = -941.4\,\text{KJ} \quad (19)$$

$$Mn + 2NaCl + O_2 = MnO + Na_2O + Cl_2 \quad \Delta G = -29.4\,\text{KJ} \quad (20)$$

$$Si + 4NaCl + 2O_2 = SiO_2 + 2Na_2O + 2Cl_2 \quad \Delta G = +25.1\,\text{KJ} \quad (21)$$

As can be seen in Table V, the dissociation pressures of Al-, Si- and Mn-oxides (MnO) are many orders of magnitude lower than those of Ni- and Cr-oxides. The resulting metal oxides generated from the above reactions would form a two-layered scale of Al_2O_3 and Mn_2O_3 with the Al_2O_3 next to the substrate as shown in Fig. 6, while Mn_2O_3 is formed from the oxidation of a *p*-type semiconductor MnO. According to our previous study [5], higher temperature enhances volume diffusion of aluminum in the alloy substrate and the outward flux of aluminum toward the scale/substrate interface, leading to the formation of the protective Al_2O_3 scale. Thus, as shown in Fig. 6, an aluminum-rich layer is able to form in the inner scale, which enables decrease in the internal penetration of chlorine produced by oxychlorination. However, some chlorine still, inevitably, attacks the alloy substrate and reacts with metals.

$$2Al + 3Cl_2 = 2AlCl_{3(g)} \quad \Delta G = -1050.4\,\text{KJ} \quad (22)$$

$$Mn + Cl_2 = MnCl_{2(l)} \quad \Delta G = -284.7\,\text{KJ} \quad (23)$$

$$Si + 2Cl_2 = SiCl_{4(g)} \quad \Delta G = -509.2\,\text{KJ} \quad (24)$$

As indicated in Table IV, the vapor pressure of $MnCl_{2(l)}$ is higher than 10^{-3} atm at 900°C and the boiling points of $AlCl_{3(g)}$ and $SiCl_{4(g)}$ are only 182°C and 58°C, respectively. Once these chlorides are formed from the above reactions, the chlorides volatilize outward to the place with appropriate partial pressure of oxygen that enables the onset of oxidation. Reactions of metal chlorides with oxygen occur.

$$4AlCl_{3(g)} + 3O_2 = 2Al_2O_3 + 6Cl_2 \quad \Delta G = -518.1\,\text{KJ} \quad (25)$$

$$2MnCl_{2(l)} + O_2 = 2MnO + 2Cl_2 \quad \Delta G = +78.6\,\text{KJ} \quad (26)$$

$$SiCl_{4(g)} + O_2 = SiO_2 + 2Cl_2 \quad \Delta G = -190.8\,\text{KJ} \quad (27)$$

Due to low dissociation pressure of Al_2O_3 and SiO_2, these oxides would be gathered in the scale/substrate interface to form a compact scale as shown in Fig. 6, preventing further chlorine attack. Consequently, the corrosion weight gain of Femnal alloy is much lower than that of 304SS.

In summary, the major difference of the effect of alloying elements on the hot corrosion behavior between 304SS and Femnal alloy is the position of oxide

formation. Owing to the rather low dissociation pressures of Al- and Si-oxides, the oxides produced by the oxychlorination and chlorination/oxidation cyclic reactions would be gathered adjacent to the alloy surface to form a thin and compact scale, preventing Femnal alloy from NaCl or Cl_2 attack effectively.

5. Conclusions

1. The initial NaCl coating accelerates oxidation of both 304 stainless steel and Fe-Mn-Al alloy at 900°C. A catalytic action of chloride is thought to be the principal cause. However, the corrosion resistance of Fe-Mn-Al alloy is superior to that of 304SS by virtue of forming a compact Al_2O_3 scale.

2. For the accelerated oxidation of 304SS, chlorides or chlorine is accumulated easily at the grain boundaries concentrated with high defects and penetrates further into the alloy substrate due to the formation of non-protective scale containing Cr_2O_3.

3. The loose and discontinuous Cr_2O_3 scale formed near the specimen's surface of 304SS is generated by the reactions between chromium chloride and oxygen. This leads to the rapid outward diffusion of iron and chromium at the grain boundaries, and the subsequent increase of nickel activity in this region results in the formation of $NiCl_{2(s)}$.

4. For an Al_2O_3-forming alloy, due to the rather low dissociation pressures of aluminum oxide, the oxide produced by the oxychlorination and chlorination/oxidation cyclic reactions would be gathered adjacent to the alloy surface to form a thin and compact scale, preventing further chlorides or chlorine attack.

Acknowledgments

The authors are grateful to the National Science of Council, Taiwan for financial support of the work under Grant No. NSC 90-2218-E-236-003 and NSC 90-2216-E-011-042. The authors would also like to thank Dr. Chin-Hai Kao for the materials support.

References

1. Y. SHINATA, F. TAKAHASHI and K. HASHIURA, *Mater. Sci. and Eng.* **87** (1987) 399.
2. M. K. HOSSAIN and S. R. J. SAUNDERS, *Oxid. Met.* **12** (1978) 1.
3. Y. SHINATA, *ibid.* **27** (1987) 315.
4. Y. SHINATA, M. HARA and T. NAKAGAWA, *Mater. Trans. JIM* **32** (1991) 969.
5. C. J. WANG and Y. C. CHANG, *Mater. Chem. Phys.* **76** (2002) 151.
6. R. SIVAKUMAR, P. K. SAGAR and M. L. BHATIA, *Oxid. Met.* **24** (1985) 315.
7. A. U. SEYBOLT, *ibid.* **2** (1970) 119.
8. G. Y. LAI, in "High-Temperature Corrosion of Engineering Alloys" (ASM International, 1990) p. 176.
9. C. J. WANG and T. T. HE, *Oxid. Met.* **58** (2002) 415.
10. J. G. DUH and C. J. WANG, *J. Mater. Sci.* **25** (1990) 2063.
11. R. D. K. MISRA and R. SIVAKUMAR, *Oxid. Met.* **25** (1986) 83.
12. E. T. TURKDOGAN, in "Physical Chemistry of High Temperature Technology" (Academic Press, New York, 1980).
13. O. KUBASCHEWSKI, C. B. ALCOCK and P. J. SPENCER, in "Materials Thermochemistry," 6th ed. (Pergamon Press, Oxford and New York, 1993).
14. O. KUBASCHEWSKI and E. L. EVANS, in "Metallurgical Thermochemistry," 2nd ed. (Wiley, New York, 1958).
15. A. ZAHS, M. SPIEGEL and H. J. GRABKE, *Corr. Sci.* **42** (2000) 1093.
16. ASM, in "Heat Treatment's Guide Standard Practices and Procedures for Steel," edited by P. M. Unterveiser, H. E. Boyer and J. J. Kubbs (ASM international, 1988) p. 410.
17. R. WANG, M. J. STRASZHEIM and R. A. RAPP, *Oxid. Mat.* **21** (1984) 71.

Received 31 July 2002
and accepted 9 June 2003